ACS APPLIED MATERIALS & INTERFACES

Research Article

www.acsami.org

Fully Enclosed Cylindrical Single-Electrode-Based Triboelectric Nanogenerator

Yuanjie Su,[†,‡,∥] Ya Yang,[†,∥] Xiandai Zhong,[§] Hulin Zhang,[†] Zhiming Wu,[‡] Yadong Jiang,[‡] and Zhong Lin Wang*[,†,§]

[†]School of Materials Science and Engineering, Georgia Institute of Technology, Atlanta, Georgia 30332-0245, United States

[‡]State Key Laboratory of Electronic Thin Films and Integrated Devices, School of Optoelectronic Information, University of Electronic Science and Technology of China (UESTC), Chengdu 610054, China

[§]Satellite Laboratory, MANA, National Institute of Materials Science, Tsukuba-city, Ibaraki 305-0047, Japan

Supporting Information

ABSTRACT: We report a fully enclosed cylindrical single-electrode-based triboelectric nanogenerator (S-TENG) consisting of a perfluoroalkoxy (PFA) ball with surface-etched nanowires, a floating latex balloon, and an Al electrode at the end of the balloon. The mechanism of the S-TENG includes two independent processes: contact-induced electrification between the PFA ball and the balloon and electrostatic induction between the charged PFA ball and the Al electrode. The relationships between the electrical outputs and the sliding distance of the PFA ball were systematically investigated by combining experimental results with finite-element calculations. The S-TENG delivers an output voltage up to 236 V and a short-circuit current of 4.8 μA, which can be used as a direct power source for driving tens of green light-emitting diodes (LEDs). The S-TENG is a potential power source for gas-flow harvesters, air navigation, and environmental monitoring.

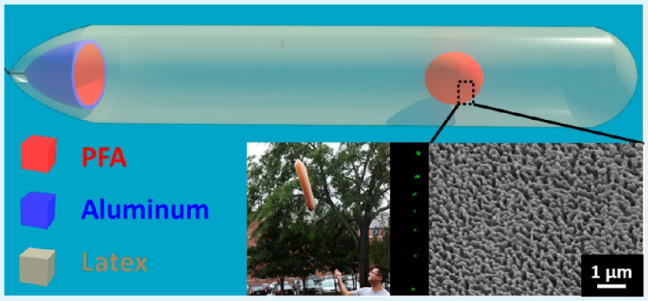

KEYWORDS: *triboelectric nanogenerator, single-electrode-based, self-powered, energy harvesting*

INTRODUCTION

Owing to the fast development of modern society and technology, energy scavenging for powering wireless, portable electronics is a new emerging area. Mechanical energy, as one of the most general power sources, is universally available in the natural environment; harvesting small-scale mechanical energy is an important part of green and renewable energy. Many kinds of mechanical-energy-harvesting technologies have been developed by utilizing electrostatic,[1−3] electromagnetic,[4,5] and piezoelectric effects.[6−9] Currently, the newly invented triboelectric nanogenerator (TENG) has been utilized to scavenge ambient mechanical energy from periodic impacts, relative sliding, and rotations, with the aim of powering micro/nanosystems,[10−13] portable electronic devices,[14,15] environmental detectors,[16,17] and sensors.[18−22] These TENGs usually need two metal electrodes deposited on the back of the triboelectric materials for the electrostatic induction and electric output, which may increase their fabrication cost and limit their application in some cases, such as a rotating tire or human skin touch. For these cases, single-electrode-based TENG (S-TENG) has been introduced for realizing a more practical and feasible design.[23,24] The advantage of the S-TENG is that there is no need for metal electrodes deposited on the triboelectric materials. The triboelectrification and the electrostatic induction of the S-TENG are achieved at the same time by the contact and separation of two triboelectric materials. There has been no report on the sequential separation of triboelectrification and electrostatic induction for energy harvesting. In this article, we fabricated a fully enclosed S-TENG, which is based on a PFA ball with surface-etched nanowires, a floating latex balloon, and an Al electrode at the end of the balloon. The S-TENG was designed by separating the triboelectrification and electrostatic induction as two separate but sequential processes. We systematically investigated the relationships between the electrical outputs and the sliding distance of the PFA ball by combining experimental results with finite-element calculations. The S-TENG floating in the air may have potential applications in self-powered gas-flow sensors, air navigation, and environmental monitoring.

EXPERIMENTAL DETAILS

Nanowire-Based Surface Modification of PFA Film. Nanowires on the surface of PFA were formed using inductively coupled plasma (ICP) reactive-ion etching. The PFA film with a thickness of 50 μm was cleaned with isopropyl alcohol and deionized water and then blown dry with nitrogen gas. In the etching process, Au particles were deposited by using dc sputter on the PFA surface as a mask.

Received: October 18, 2013
Accepted: December 11, 2013
Published: December 11, 2013

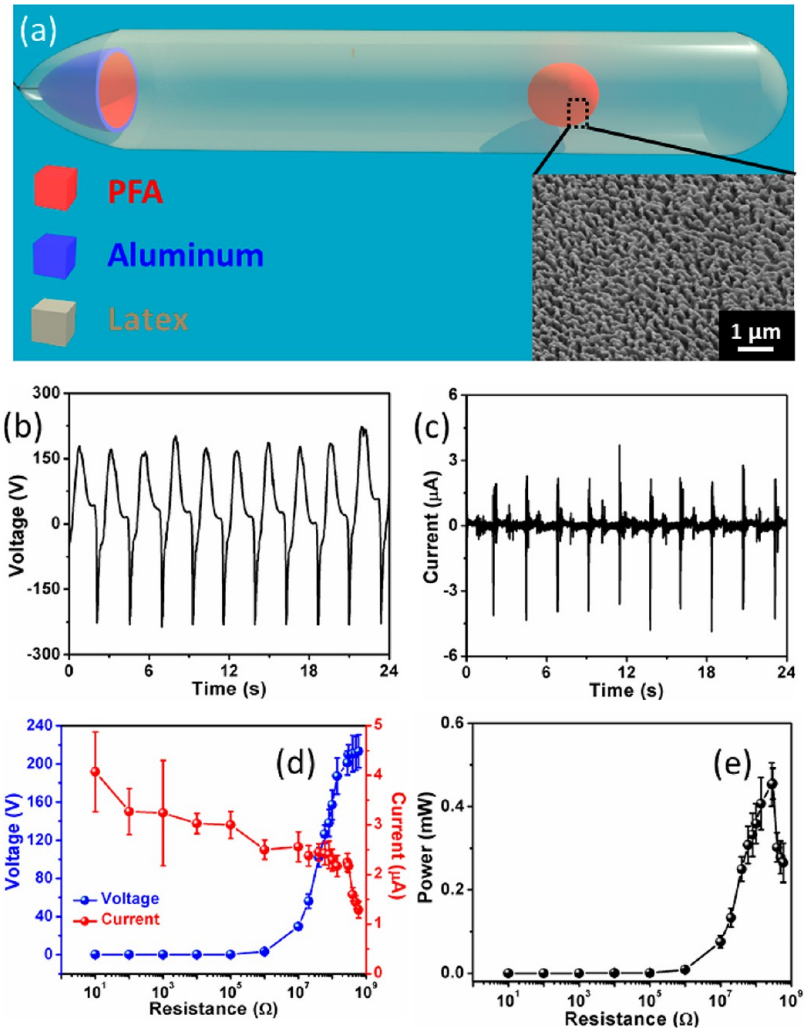

Figure 1. (a) Schematic diagram of the fabricated fully enclosed cylindrical S-TENG. Inset: SEM image of the PFA surface with the etched nanowire structure at the tilted view of 30°. (b) Output voltage and (c) short-circuit current (I_{sc}) of the S-TENG. (d) Dependence of the output voltage and current on the external loading resistance. (e) Plot of the power density versus the loading resistance.

Subsequently, a mixed gas including Ar, O_2, and CF_4 was introduced in the ICP chamber, with corresponding flow rates of 15.0, 10.0, and 30.0 sccm, respectively. The PFA film was etched for 15 s to obtain the nanowire structure on the surface. One power source of 400 W was used to yield a large density of plasma, whereas another 100 W power source was used to accelerate the plasma ions.

Fabrication of a Fully Enclosed S-TENG. The fully enclosed cylindrical S-TENG consists of a PFA film-based ball, a latex balloon, and Al foil as an electrode. The latex balloons were purchased from Qualatex. Helium gas was used to inflate the balloon. A rubber ball (6 cm) was wrapped with etched PFA film on the surface. Al foil with an area of 76.9 cm^2 was attached to a transparent acrylic hemisphere to form a bowl-shaped electrode for the purpose of electrostatic induction, and the PFA film was then covered on the surface of the Al electrode.

Characterization and Electrical Measurement of the S-TENG. One end of the TENG with the Al electrode was fixed on a foam bulk, and the other end was lifted into a vertical position and laid down to a horizontal position during the electrical measurement. The morphology and nanostructure of the etched PFA film were characterized by Hitachi SU8010 field-emission scanning electron microscopy (SEM) operated at 5 kV. The output performance of the TENG was measured using Stanford Research Systems SR560 and SR570 low-noise current amplifiers to record the voltage and current, respectively.

RESULTS AND DISCUSSION

The fabricated S-TENG has a fully enclosed structure with a PFA-film-based plastic ball and an Al electrode in a latex balloon, as displayed in Figure 1a. PFA and latex were selected as the triboelectric materials because of their large difference in their ability to lose electrons in triboelectric series.[25] The bowl-shaped Al electrode was used to transfer electrons between Al and ground, where the Al electrode was covered by a layer of PFA to prevent the direct contact and friction between the PFA ball and Al electrode. Thus, the electrostatic induction and generation of triboelectric charges in the device are separated and independent. As depicted in the inset of Figure 1a, the PFA film surface was etched into nanowire structures with a length of 340 nm and diameters ranging from 70 to 110 nm. The etched nanowires on the surface of PFA can enhance the triboelectric charge density because of the increase in the effective contact area in the friction process.[26] Figure 1b,c shows the output performance of the S-TENG, where the output voltage can reach 236 V with a peak short-circuit current of 4.8 μA. In general, the effective output performance of the TENG relies on the match with the loading resistance. Figure 1d illustrates the plot of the output voltage and output current as a function of the external loading resistance. The output

dx.doi.org/10.1021/am404611h | ACS Appl. Mater. Interfaces 2014, 6, 553−559

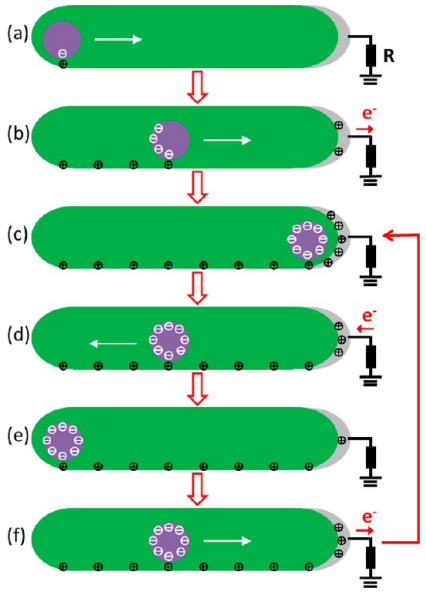

Figure 2. Working mechanism of the fully enclosed cylindrical S-TENG. (a) Initial contacting position. (b) Electrification between PFA and latex as the ball rolls toward the Al electrode. (c) PFA ball with saturated and uniform triboelectric charges at the closest position. (d) Rolling away from the Al electrode. (e) Farthest position of the ball. (f) Rolling toward the Al electrode.

voltage rises with the increasing loading resistance, whereas the current through the loading resistance follows the opposite trend and drops with an increase of the resistance. As displayed in Figure 1e, with increasing loading resistance, the instantaneous power stays close to 0 with the resistance below 1 MΩ and then goes up as the resistance increases from 1 to 300 MΩ. Subsequently, the power decays under a resistance larger than 300 MΩ. Therefore, the maximum value of the output power can reach 0.445 mW at a loading resistance of 300 MΩ.

The mechanism of the fully enclosed S-TENG is schematically depicted in Figure 2. In the original position, the surfaces of PFA and latex are in contact with each other, as illustrated in Figure 2a. Because of the large difference in the triboelectric series,[27] the PFA film attracts and retains electrons from latex, leaving net positive charges on the latex surface and equal net negative charges on the PFA surface. The generated negative triboelectric charges can be maintained on the PFA surface for a long time owing to the insulating nature of the polymer materials.[28] Once the PFA ball starts to roll, the other parts on the surface will contact the latex and attract more triboelectric charges from latex surface, where the triboelectric charge density continues to increase and reaches saturation with uniform distribution along the latex and PFA, as described in Figure 2b,c. Moreover, the PFA-covered ball rolls in the balloon with uniform and constant charge quantity. As the negatively charged ball moves away from the Al electrode, the quantity of

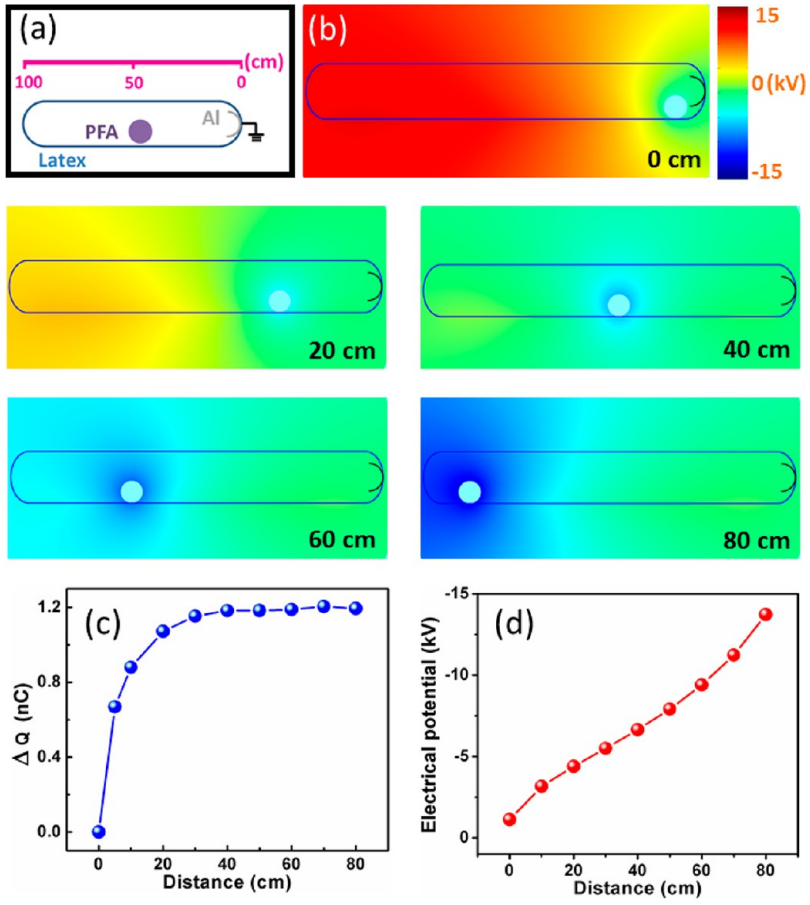

Figure 3. (a) Model of the fabricated S-TENG for the calculation. (b) Finite-element simulation of the potential distribution in the S-TENG. (c) Plot of transferred induced charge quantity, ΔQ, on the Al electrode versus the distance between PFA and Al. (d) Curve of the simulated potential versus the distance between PFA and Al.

dx.doi.org/10.1021/am404611h | ACS Appl. Mater. Interfaces 2014, 6, 553−559

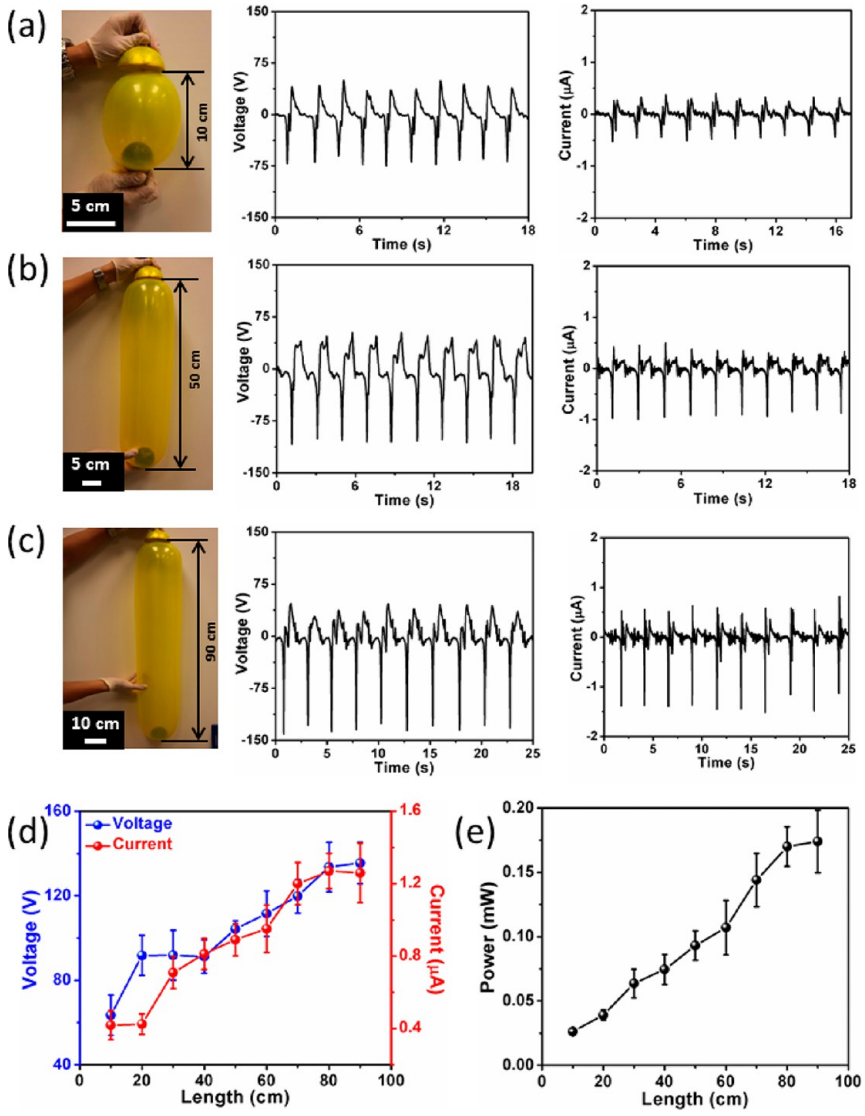

Figure 4. Photograph and electric output of the fully enclosed S-TENG with a working length of (a) 10, (b) 50, and (c) 90 cm. (d, e) Dependence of (d) electric output and (e) instantaneous power on the working length.

induced positive charges on Al foil surface will decrease, resulting in electrons flowing from the ground to Al, as represented in Figure 2d. When the PFA ball reaches the farthest point, the quantity of induced charges on the Al foil surface reaches a minimum, and no more electrons are transferred between the ground and Al, as displayed in Figure 2e. As the ball moves toward the Al electrode, the quantity of induced charges will increase, driving electrons to flow from the Al electrode to ground, as shown in Figure 2f. Once the ball reaches the point nearest to the Al electrode, the induced charge quantity on the surface of the Al foil will reach its maximum again, as depicted in Figure 2c. In this entire cycle, the PFA ball with negative triboelectric charges moves back and forth in the device, producing an alternating electric output on the external load in Figure 1b,c.

The electrical-potential distribution and charge-transfer process in the S-TENG can be verified through numerical simulation using COMSOL. The proposed model is based on a PFA ball with a diameter of 6 cm and a bowl-shaped Al foil with diameter of 7.5 cm in the enclosed latex cylinder with the same dimensions ($90 \times 14 \times 1\ 4\ cm^3$), as represented in Figure 3a. The quantities of the triboelectric charges on the surfaces of the PFA ball and the latex balloon with the length direction were assumed to be −188.4 and +188.4 nC, respectively. The Al foil was connected with the ground. Figure 3b depicts the calculated results of the electrical-potential distribution caused by electrostatic induction in the device under five different distances: 0, 20, 40, 60, and 80 cm. When the PFA ball rolls away from Al to a distance of 20 cm, the electric potential on the PFA surface increases to −4384 V. It can be clearly seen that the potential difference between the PFA and Al increases dramatically with increasing distance and reaches a maximum value of -1.37×10^4 V at a distance of 80 cm, as revealed in Figure 3d (Figure S1, Supporting Information). However, the amount of the transferred induced charges (ΔQ) on the Al electrode increases with increasing distance and saturates at distance of 40 cm, as exhibited in Figure 3c, implying that electrons flow from the ground to the Al electrode when the PFA ball departs from the Al electrode.

A systematic investigation of the relationship between the electric output and the working length of the device was carried out experimentally. The electric output was measured under a

dx.doi.org/10.1021/am404611h | ACS Appl. Mater. Interfaces 2014, 6, 553−559

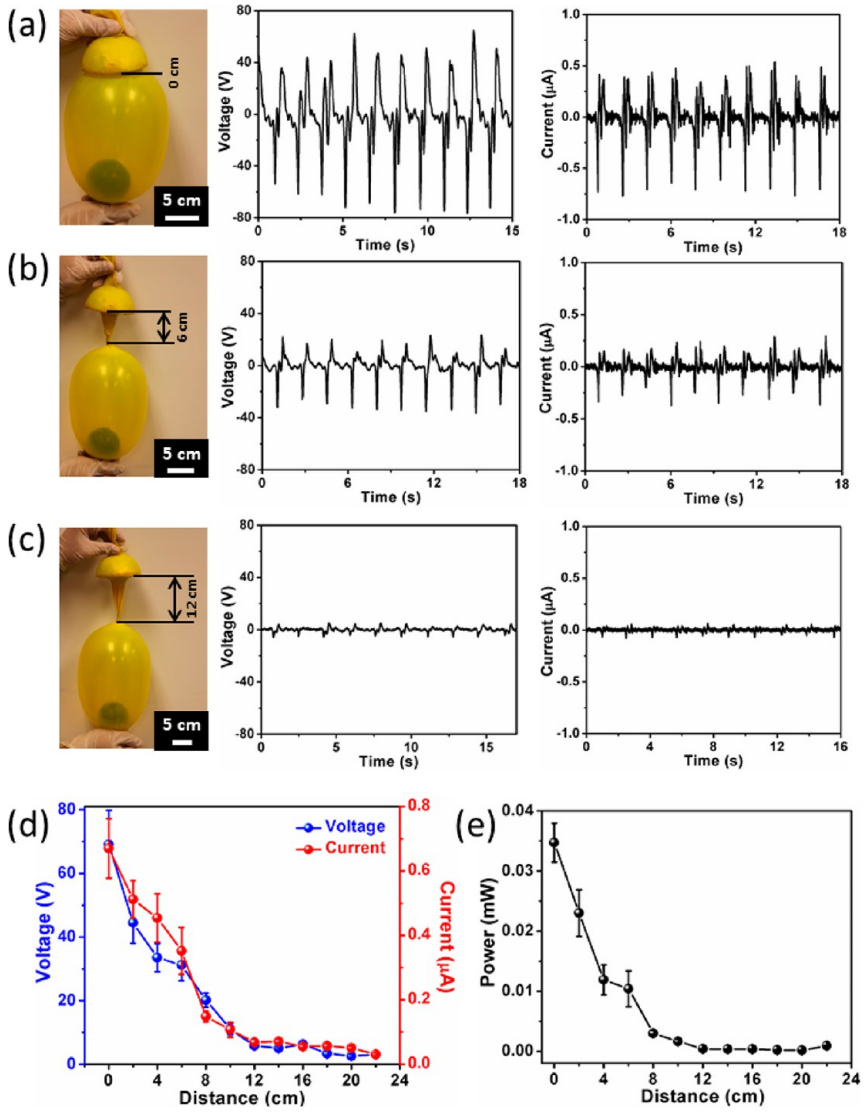

Figure 5. Photograph and electric output of the fully enclosed S-TENG with a induction distance of (a) 0, (b) 6, and (c) 12 cm. (d, e) Dependence of (d) electric output and (e) instantaneous power on the induction distance.

series of nine different working lengths from 10 to 90 cm by an electrometer with a load of 300 MΩ. To avoid the triboelectric effect between the PFA ball and Al electrode, the bowl-shaped electrode and PFA ball were spaced apart by wringing the balloon to create another enclosed space for the ball, as shown in the photographs in Figure 4. As the PFA ball rolls toward the Al electrode in the balloon under a length of 10 cm, an output voltage of −63.5 V can be observed, indicating the induced potential difference between PFA and Al. Furthermore, the transfer of the charges between the Al electrode and ground in the external circuit generates an alternating current with a negative peak of −0.53 μA and a positive peak of 0.43 μA, as illustrated in Figure 4a. At a longer working length, the fabricated TENG yields a larger output voltage and current, as illustrated in Figure 4b,c, because the electric output mainly depends on the electrical-potential difference between the PFA and Al, which is proportional to the working distance, as shown in Figure 3d. The output voltage and current follow a similar tendency as the potential difference and increase with the increasing working length. Furthermore, the output current is also associated with the movement speed of the PFA ball. Because of gravitational force, the ball moves faster in the device with a longer working length, leading to a higher speed at the collision or shorter approaching time and thus a larger electric output. This is further confirmed by the results in Figure 4d where both the output voltage and output current of the S-TENG are enhanced with a longer working length (Figures S2 and S3, Supporting Information). Consequently, the instantaneous power output is proportional to the working length of the S-TENG, as shown in Figure 4e.

It should be noted that the designed S-TENG is based on a single-electrode structure in which the Al electrode was connected to the ground. Because of electrostatic induction, the quantity of induced charges on the metal is largely dependent on the induction distance. To investigate the relationship between the induction distance and the electrical output performance, the fabricated S-TENG was divided into an electrode part and an inflated part with a fixed length of 20 cm for the movement of the PFA ball, where the distance between the two parts can be modulated, as presented in Figure 5. When the two parts contact each other (Figure 5a), the PFA ball rolls backward and forward in the inflated part of the

dx.doi.org/10.1021/am404611h | ACS Appl. Mater. Interfaces 2014, 6, 553−559

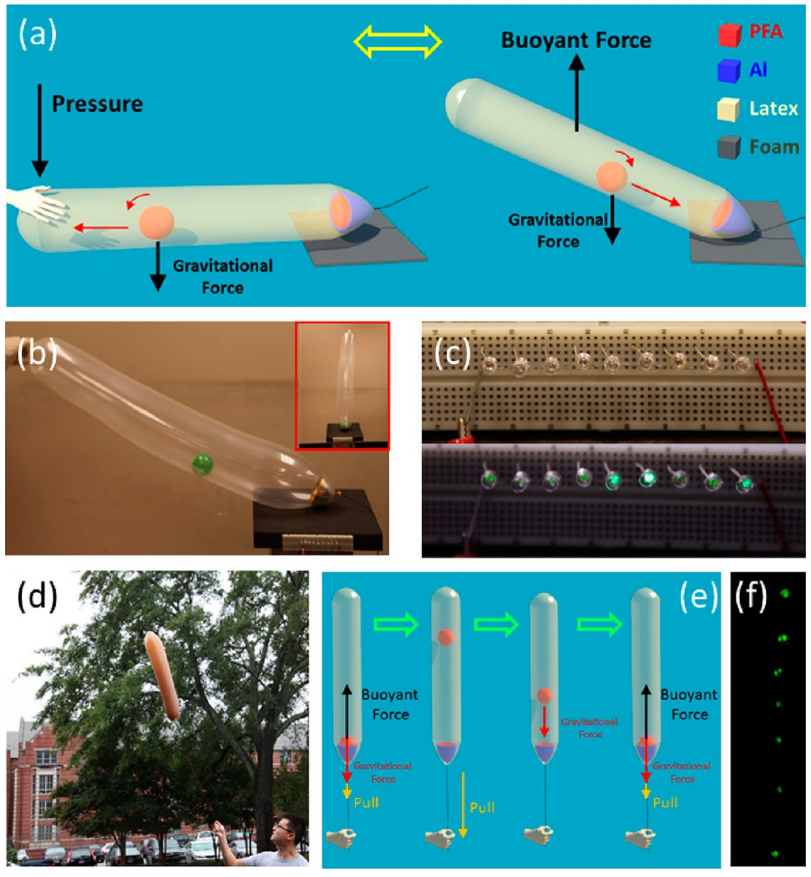

Figure 6. (a) Schematic diagram and (b) photograph of the fabricated S-TENG. (c) Snapshot of green LEDs directly driven by the S-TENG. (d) Photograph of the floating S-TENG filled with helium gas. (e) Operation cycle of the floating S-TENG. (f) Photograph of green LEDs lit by the floating S-TENG.

balloon, producing an output voltage up to 69.1 V and a current of 0.67 μA. With increasing distance between the two parts, the S-TENG delivers a lower electric output, as displayed in Figure 5b,c. It can be clearly seen that the output voltage and current at a distance of 12 cm are almost negligible as compared with the electrical-output performance at the original position. Under a fixed working length of 20 cm in the S-TENG, the average peak output voltages and currents at different distances were extracted and are shown in Figure 5d, distinctly indicating that the increase in the distance between the PFA ball and Al electrode results in a monotonic decrease in both the output voltage and current that is dramatic (Figures S4 and S5, Supporting Information). The movement of the charged PFA ball can barely cause a change in the induction charges on the surface of Al when the induction distance surpasses a certain value. Because it is dominated by the decrease of the output voltage and current, the generated instantaneous power of the S-TENG shows a significant decaying trend and drops by about 98% under an induction distance of 12 cm, as displayed in Figure 5e.

To verify the capability of the fully enclosed cylindrical S-TENG to be an effective power source, two sets of practical applications were demonstrated, where helium gas was injected into the balloon to generate a buoyant force to ensure that the balloon can return back to its original position when triggered by external impacts in the process of mechanical-energy harvesting. As illustrated in Figure 6a, the S-TENG with one end fixed on the foam was pressed down to a horizontal position, leaving the PFA ball rolling toward the Al electrode and driving the electrons to flow from the ground to the electrode. When the applied force was removed, the buoyant force lifts the unfixed part of balloon. Thus, as displayed in Figure 6b, the PFA ball rolls back to the bowl-shaped Al electrode as a result of gravitational force, which drives the electrons to flow from the electrode to the ground (Figure S6, Supporting Information). By repeating this operation cycle, the S-TENG can be used to directly light up nine green light-emitting-diode (LEDs) simultaneously, as depicted in Figure 6c. In the second demonstration, enough Helium gas was injected into the balloon so that the device can overcome the gravitational force and move up in the air, as illustrated in Figure 6d. The corresponding electric-energy-generation process of the S-TENG is elaborated in Figure 6e. At its original position, the S-TENG is maintained in the air, allowing contact between the PFA ball and the Al electrode. When an external impact is applied to the balloon, the PFA ball is retained in its original place at that time, whereas the Al electrode moves down suddenly because of a pulling force. Thus, a relative separation between the PFA ball and electrode was created, leading to a decrease in the induced positive charges on the Al electrode. Subsequently, the PFA ball then falls toward the Al electrode because of gravitational force, resulting in an increase in the amount of the inductive positive charges. Once the ball drops on the Al electrode, a new equilibrium among the buoyant force, gravitational force, and pulling force will be reached again, resulting in the S-TENG returning back to its original state (Figure S7, Supporting Information). To illustrate the electric-output performance of

the fully enclosed S-TENG in this working cycle, seven green light-emitting-diodes (LEDs) were lit simultaneously, as displayed in Figure 6f. This demonstration indicates that the fabricated S-TENG is capable of converting slight movement and vibration in the air to electricity, paving the way for potential applications in self-powered systems, gas-flow harvesters, environmental detectors, weather sensors, and air navigation.

CONCLUSIONS

We have demonstrated a fully enclosed cylindrical S-TENG consisting of a PFA ball with surface-etched nanowires, a floating latex balloon, and an Al electrode. The mechanism of the S-TENG is based on both contact-induced electrification and electrostatic induction, which occur in sequence rather than in parallel. The relationship between the electric output and the working length was systematically studied by both numerical simulation and experimental measurement. The designed S-TENG has potential applications in self-powered weather sensors, air-flow detectors, and environmental monitoring.

ASSOCIATED CONTENT

Supporting Information

Finite-element simulation of the potential distribution in S-TENG by COMSOL, electric output of the S-TENG under various working lengths and distances, and photographs of the working cycle of the device. This material is available free of charge via the Internet at http://pubs.acs.org.

AUTHOR INFORMATION

Corresponding Author

*E-mail: zlwang@gatech.edu.

Author Contributions

[‖]These authors contributed equally to the work.

Notes

The authors declare no competing financial interest.

ACKNOWLEDGMENTS

This work was supported by the U.S. Airforce, MURI, U.S. Department of Energy, Office of Basic Energy Sciences (DE-FG02-07ER46394), MANA, National Institute of Materials Science, Japan, and the "Thousands Talents" program for a pioneer researcher and his innovation team, China. Y.J.S., Z.M.W., and Y.D.J. acknowledge support from the National Science Foundation of China via grant no. 61101029. Y.J.S. also acknowledges a fellowship from the China Scholarship Council (CSC).

REFERENCES

(1) Herb, R. G.; Parkinson, D. B.; Kerst, D. W. *Phys. Rev.* **1937**, *51*, 75−83.
(2) Mitcheson, P. D.; Miao, P.; Stark, B. H.; Yeatman, E. M.; Holmes, A. S.; Green, T. C. *Sens. Actuators, A.* **2004**, *115*, 523−529.
(3) Miao, P.; Mitcheson, P. D.; Holmes, A. S.; Yeatman, E. M.; Green, T. C.; Stark, B. H. *Microsyst. Technol.* **2006**, *12*, 1079−1083.
(4) Rome, L. C.; Flynn, L.; Goldman, E. M.; Yoo, T. D. *Science* **2005**, *309*, 1725−1728.
(5) Williams, C. B.; Shearwood, C.; Harradine, M. A.; Mellor, P. H.; Birch, T. S.; Yates, R. B. *IEE Proc.: Circuits Devices Syst.* **2001**, *6*, 337−342.
(6) Wang, Z. L.; Song, J. H. *Science* **2006**, *312*, 242−246.
(7) Liu, J. M.; Wu, W. W.; Bai, S.; Qin, Y. *ACS Appl. Mater. Interfaces* **2011**, *3*, 4197−4200.
(8) Velazquez, J. M.; Baskaran, S.; Gaikwad, A. V.; Ngo-Duc, T. T.; He, X. T.; Oye, M. M.; Meyyappan, M.; Rout, T. K.; Fu, J. Y.; Banerjee, S. *ACS Appl. Mater. Interfaces* **2013**, *5*, 10650−10657.
(9) Bester, G.; Wu, X. F.; Vanderbilt, D.; Zunger, A. *Phys. Rev. Lett.* **2006**, *96*, 187602-1−187602-4.
(10) Tian, H.; Ma, S.; Zhao, H. M.; Wu, C.; Ge, J.; Xie, D.; Yang, Y.; Ren, L. T. *Nanoscale* **2013**, *5*, 8951−8957.
(11) Lowell, J.; Rose-Innes, A. C. *Adv. Phys.* **1980**, *29*, 947−1023.
(12) Zhang, X. S.; Han, M. D.; Wang, R. X.; Zhu, F. Y.; Li, Z. H.; Wang, W.; Zhang, H. X. *Nano Lett.* **2013**, *13*, 1168−1172.
(13) Meng, B.; Tang, W.; Zhang, X. S.; Han, M. D.; Liu, W.; Zhang, H. X. *Nano Energy* **2013**, *6*, 1101−1106.
(14) Castle, P. G. *J. Electrost.* **1997**, *40−1*, 13−20.
(15) Zhu, G.; Yang, R.; Wang, S.; Wang, Z. L. *Nano Lett.* **2010**, *10*, 3151−3155.
(16) Lee, M.; Bae, J.; Lee, J.; Lee, C.-S.; Hong, S.; Wang, Z. L. *Energy Environ. Sci.* **2011**, *4*, 3359−3363.
(17) Su, Y. J.; Yang, Y.; Zhang, H. L.; Xie, Y. N; Wu, Z. M.; Jiang, Y. D.; Fukata, N.; Bando, Y.; Wang, Z. L. *Nanotechnology* **2013**, *24*, 295401.
(18) Beeby, S. P.; Tudor, M. J.; White, N. M. *Meas. Sci. Technol.* **2006**, *17*, 175−95.
(19) Round, S.; Steingart, D.; Frechette, L.; Wright, P.; Rabaey, J. *Lect. Notes Comput. Sci. Eng.* **2004**, *920*, 1−17.
(20) Shen, G. P.; Qin, M.; Huang, Q.-A. *IEEE Sens. J.* **2010**, *10*, 340−346.
(21) Meng, B.; Tang, Wei.; Too, Z. H.; Zhang, X. S.; Han, M. D.; Liu, W.; Zhang, H. X. *Energy Environ. Sci.* **2013**, *6*, 3235−3240.
(22) Tang, W.; Meng, B.; Zhang, H. X. *Nano Energy.* **2013**, *2*, 1164−1171.
(23) Yang, Y.; Zhang, H. L.; Lin, Z. H.; Zhou, Y. S.; Jing, Q. S.; Su, Y. J.; Yang, J.; Chen, J.; Hu, C. G.; Wang, Z. L. *ACS Nano* **2013**, *7*, 9213−9222.
(24) Maheshwari, V.; Saraf, R. F. *Science* **2006**, *312*, 1501−1504.
(25) McCarty, L. S.; Whitesides, G. M. *Angew. Chem., Int. Ed.* **2008**, *47*, 2188−2207.
(26) Yang, Y.; Zhang, H.; Lee, S.; Kim, D.; Hwang, W.; Wang, Z. L. *Nano Lett.* **2013**, *13*, 803−808.
(27) Shashoua, V. E. *J. Polym. Sci.* **1958**, *33*, 65−85.
(28) Saurenbach, F.; Wollmann, D.; Terris, B. D.; Diaz, A. F. *Langmuir* **1992**, *8*, 1199−1203.